ADVANCED MATERIALS
www.advmat.de

Hydrogel-Impregnated Robust Interlocking Nano Connector (HiRINC) for Noninvasive Anti-Migration of Esophageal Stent

Eunyoung Jeon, Song Hee Kim, Sukyoung Kim, Dae Sung Ryu, Ji Won Kim, Kayoung Kim, Do Hoon Kim, Jung-Hoon Park, and Joonseok Lee**

Migration of implanted self-expandable metallic stent (SEMS) in the malignant or benign esophageal stricture is a common complication but not yet resolved. Herein, this research develops a hydrogel-impregnated robust interlocking nano connector (HiRINC) to ensure adhesion and reduce the mechanical mismatch between SEMSs and esophageal tissues. Featuring a network-like porous layer, HiRINC significantly enhances adhesion and energy dissipation during esophageal peristalsis by utilizing mechanical interlocking and increasing hydrogen bonding sites, thereby securing SEMS to tissues. The anti-swelling property of HiRINC prevents excessive hydrogel expansion, avoiding esophageal blockage. Ex vivo and in vivo adhesion tests confirm that the HiRINC outperforms flat surfaces without RINC structures and effectively prevents stent migration. HiRINC-coated SEMS maintains its position and luminal patency, minimizing stent-induced tissue hyperplasia and inflammatory responses in rat and porcine esophageal models during the 4-week follow-up. This novel HiRINC-SEMS can ensure anti-migration and prolonged stent patency in the rat and porcine esophagus and seems to be expanded to other nonvascular luminal organs and various implantable metallic devices.

1. Introduction

Gradual narrowing of the esophageal lumen, caused by malignant and benign esophageal strictures, results in severe dysphagia. This condition impairs the ability of the patient to swallow aliment, adversely affecting nutritional status and quality of life.[1] Pathologies such as gastric, lung, breast, and mediastinal cancers can also cause dysphagia by externally compressing esophageal lumen.[2] Retrievable or nonretrievable SEMSs have been used as a leading palliative treatment for the dysphagia resulting from esophageal strictures. Various types such as fully covered, partially covered, or uncovered SEMS are used depending on whether the disease is malignant or benign. The SEMSs have been extended to a variety of nonvascular luminal organs including the esophagus, gastroduodenum, colorectum, pancreaticobiliary, airway, and urinary tract.[3] However, early complications of esophageal stent placement have been included chest pain, fever, bleeding, foreign body sensation, and stent migration. Furthermore, delayed stent-in-restenosis leading to recurrent dysphagia symptom caused by tumor or granulation tissue growth, esophagorespiratory fistula formation, and food impaction can occur after stent placement.[4] Among them, stent

E. Jeon, S. Kim, J. Lee
Department of Chemistry
Hanyang University
Seoul 04763, Republic of Korea
E-mail: joonseoklee@hanyang.ac.kr

S. H. Kim, D. S. Ryu, J. W. Kim, J.-H. Park
Department of Convergence Medicine
Asan Medical Center
University of Ulsan College of Medicine
88 Olympic-ro 43-gil, Songpa-gu, Seoul 05505, Republic of Korea
E-mail: jhparkz@amc.seoul.kr

The ORCID identification number(s) for the author(s) of this article can be found under https://doi.org/10.1002/adma.202414944

DOI: 10.1002/adma.202414944

S. H. Kim, D. S. Ryu, J. W. Kim, J.-H. Park
Biomedical Engineering Research Center
Asan Institute for Life Sciences
Asan Medical Center
88 Olympic-ro 43-gil, Songpa-gu, Seoul 05505, Republic of Korea

K. Kim
Department of Fiber Convergence Material Engineering
Dankook University
Gyeonggi-Do 16890, Republic of Korea

D. H. Kim
Department of Gastroenterology
Asan Medical Center
University of Ulsan College of Medicine
88 Olympic-ro 43-gil, Songpa-gu, Seoul 05505, Republic of Korea

J. Lee
Research Institute for Convergence of Basic Sciences
Hanyang University
Seoul 04763, Republic of Korea

E. Jeon, J. Lee
VN Inc
Seoul 04763, Republic of Korea

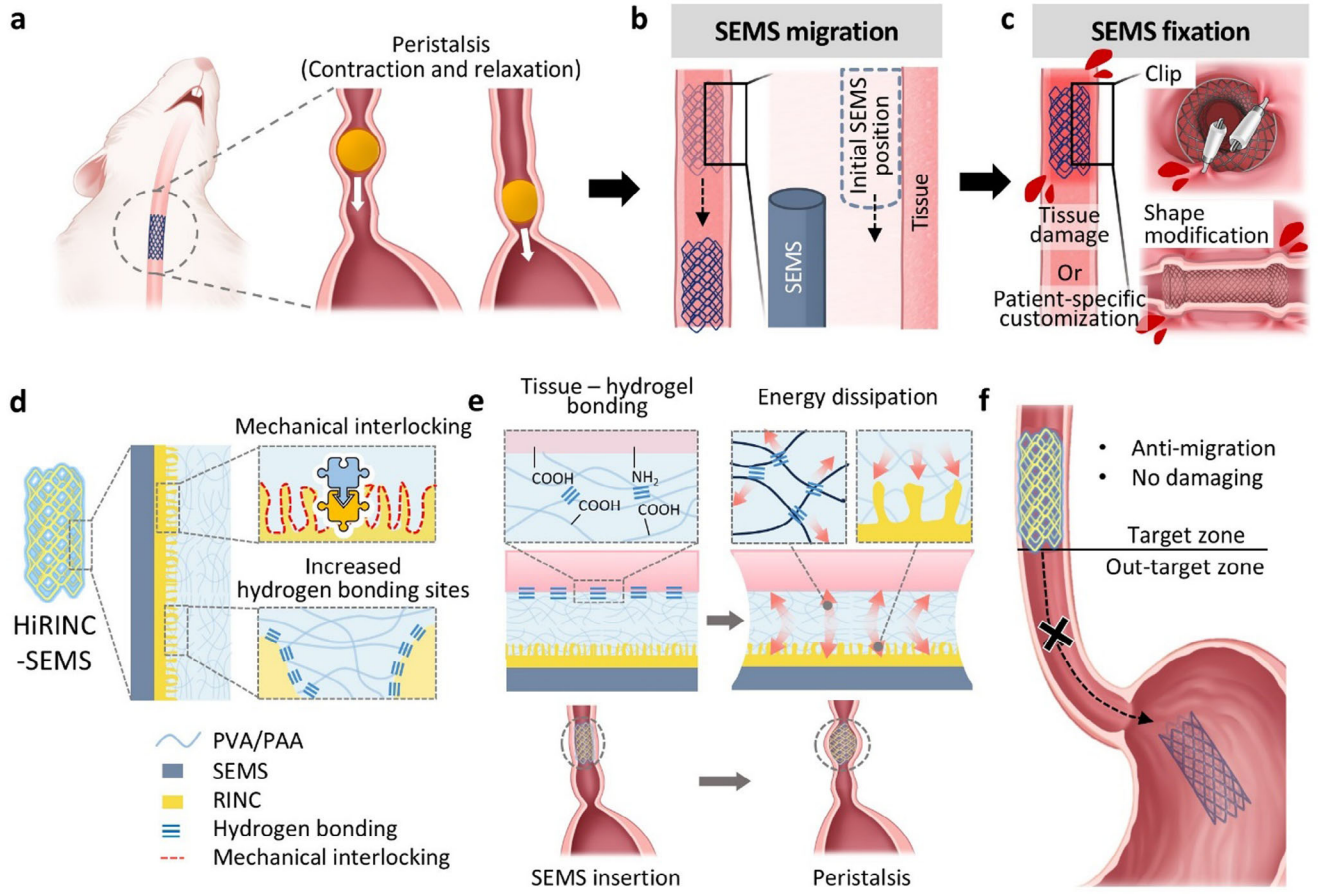

Figure 1. Development of hydrogel-impregnated robust interlocking nano connector-coated self-expandable metallic stent (HiRINC-SEMS) for anti-migration. Schematic illustrations showing a) the peristalsis mechanism in the esophagus, b) the migration of SEMS from its initial position within the esophageal tissue, and c) the conventional method of SEMS fixation to prevent SEMS migration. Schematic illustrations showing; d) the adhesion enhancement mechanism HiRINC-SEMS, highlighting the role of RINC as a network-like porous silica layer in facilitating robust adhesion; e) hydrogen bonding of tissue-adhesive hydrogel and energy dissipation within the HiRINC; and f) prevention of SEMS migration in the target zone without causing damage.

migration is the most common compilation, occurring at a range of 7–75% after esophageal stent placement.[5]

During physiological activities such as esophageal peristalsis (**Figure 1a**), the soft and moist human tissues might not align well with the rigid and dry components of conventional solid stents,[6] thereby increasing the risk of stent migration from its initial position (Figure 1b). Stent migration significantly reduces therapeutic outcomes and necessitates additional interventions, including stent removal, repositioning, and reinsertion.[7] Several anti-migration strategies have been developed, which include using endoscopic clips or suturing, modifying stent shape by expanding its size,[8] and applying double-layering techniques (Figure 1c).[8c–e,9] While endoscopic clips or suturing can secure stents, these methods are relatively invasive and can rarely damage to esophageal tissue, leading to severe complications including infection (1.2–1.8%), esophageal perforation (0.3–1.1%), and chronic inflammation (2.8–3.5%).[10] Although shape modification techniques minimize tissue damage, their applicability varies based on patient condition and stent type used, often requiring patient-specific customization. Customization, however, can be time-consuming, expensive for mass production, and impractical in emergency scenarios.[11] Although various anti-migration strategies have been suggested, gold standard for overcoming stent migration is still not established in clinical practice.

Nondamaging and simple fixation techniques are needed to overcome complications associated with conventional anti-migration methods.[12] Cyanoacrylate glue is among the strongest adhesives, but its use is limited owing to its cytotoxicity, incompatibility with wet surfaces (as it solidifies upon contact with water), and tendency to form rigid plastics that do not accommodate tissue movements.[13] Bioadhesive materials such as hydrogels are promising alternatives, offering high water content and mechanical properties that closely mimic biological tissues.[14] Carboxylic acid or *N*-hydroxysuccinimide (NHS) ester groups in hydrogels enhance tissue adhesion through physical and covalent cross-linking,[12c,15] offering biocompatibility, nontoxicity, and ease of use as suture alternatives; they enable immediate, noninvasive bonding and reduce inflammation risks. These hydrogels closely resemble natural tissues in softness and elasticity, allowing them to dissipate energy during esophageal movements.[16] Despite these advantages, their broader medical applications are limited owing to the difficulty in forming strong

bonds with solid materials such as medical devices.[17] Previous research has focused on surface functionalization to introduce functional groups that complement coupling agents on the substrate surface, but this approach limits versatility and relies heavily on specific chemicals.[18] Consequently, versatile and robust methods for durable bonding between hydrogels and solid materials are crucial for practical use.[16c]

We aimed to develop a hydrogel-impregnated robust interlocking nano connector (HiRINC) on SEMS to connect hydrogel and extra-luminal stent strut surface. The network-like porous structure of robust interlocking nano connector (RINC) increased bonding sites, enabling enhanced mechanical interlocking and hydrogen bonding with hydrogel. These synergetic effects improved the adhesion stability of SEMS (Figure 1d). At the tissue-hydrogel interface, hydrogen bonding and covalent cross-linking provided a strong and durable attachment, securing stent placement. Furthermore, the hydrogel of HiRINC dissipated energy during peristalsis by absorbing and distributing mechanical forces, reducing stress on surrounding tissues and minimizing damage during dynamic movements (Figure 1e). Ultimately, HiRINC-SEMS successfully remained within the designated target zone, effectively preventing migration to the out-target zone (Figure 1f). A 4-week follow-up in both rat and pig esophageal models further confirmed that the stent did not move, highlighting the efficacy of HiRINC-SEMS in maintaining its position over an extended duration.

2. Results and Discussion

2.1. Fabrication and Characterization of RINC and HiRINC

The RINC was fabricated on flat substrates (Si wafer and nitinol plate; hereafter, "FLAT") (**Figure 2a**) and used as control. First, an ultrathin silica seed layer with spherical small pores (≈2 nm in size) was uniformly grown on the entire substrate using small cetyltrimethylammonium cation micelles as templates (Figure S1a, Supporting Information). Subsequently, a network-like porous layer was formed, which emerged as the micelles expanded using salicylate anion.[19] Grazing-incidence small-angle X-ray scattering (GISAXS) data confirmed the presence of the seed layer during the growth process (Figure 2b). As the porous layer grew over time in the presence of a seed layer, the intensity decreased, and the lowest intensity was observed when the film did not have a seed layer. The porous layer (150 nm thick with pore size of ≈50 nm) was more robustly supported when the seed layer surrounded the substrate compared to when seed layer was absent (Figure S1b, Supporting Information). The RINC with the seed layer on the nitinol plate exhibited a higher bonding energy for Ti (from the substrate)-O-Si (from RINC) compared to the structure without the seed layer, indicating that the seed layer played a critical role in anchoring the RINC firmly to the substrate (Figure 2c).[20]

After confirming the successful fixation of the RINC on the substrates, a hydrogel layer was formed, which would adhere to esophageal tissues. We treated the RINC surfaces with hydrogel precursors using methods inspired by the interlocking mechanisms of jigsaw puzzle pieces, such as mold-casting, spin-coating, and dip-coating, depending on the specific requirements of each experiment. Details are provided in the Experimental Section, with dip-coating ultimately selected for the SEMS application. This procedure effectively filled the open pores of the RINC, resulting in a hydrogel-impregnated RINC system (hereafter, HiRINC). Figure 2d,e shows the direct contact and mechanical interlocking between the hydrogel and RINC.[21] We compared HiRINC to a hydrogel-coated flat surface (hereafter, HFLAT) to assess the role of the RINC as a hydrogel-substrate connector.

The molecular bonding characteristics were assessed using Fourier transform infrared (FT-IR) spectra (Figure 2f). HFLAT exhibited strong intramolecular bonds within the hydrogel at 3200 cm^{-1} but showed weaker intermolecular bonds at 3400 cm^{-1}, suggesting limited interaction between the hydrogel and silanol.[22] Meanwhile, HiRINC exhibited strong intermolecular bonds, indicating a more robust interaction between the hydrogel and silanol due to its high surface area. Furthermore, X-ray photoelectron spectroscopy depth profiles revealed a higher O 1s peak intensity for HiRINC, indicating the increased presence of silanol hydrogen bonding (Figure S2, Supporting Information). The mechanical interlocking and hydrogen bonding of HiRINC contribute to the robust adhesion between the hydrogel and RINC.[23]

To evaluate the adhesive properties of HiRINC, we measured its interfacial strength, adhesion strength, and work of adhesion (Figures 2g and S3, Supporting Information). During 90° peel tests, HiRINC exhibited an interfacial strength of 7.6 N cm^{-1}, which was about 126-fold greater than the interfacial strength of 0.06 N cm^{-1} for HFLAT. This notable difference indicates stronger interfacial adhesion of HiRINC, which can be attributed to its network-like porous layered structure. Lap-shear tests supported these results, with HiRINC exhibiting adhesion strength of 145 kPa compared to 8.67 kPa for HFLAT, indicating a 16-fold increase. Furthermore, the work of adhesion (represented by a larger area under the force-displacement curve) for HiRINC demonstrated a 65-fold increase to 1.63 MPa mm^{-1} when compared to 0.025 MPa mm^{-1} for HFLAT. Hence, a greater amount of energy is required to detach the hydrogel from HiRINC.[16a] HiRINC forms a robust bond, allowing the hydrogel to effectively dissipate energy and withstand stress when external forces are applied.[16b,c,24] Consequently, the hydrogel can endure high force until it exceeds the toughness threshold, resulting in cohesive failure. Contrastingly, the weak bonding of HFLAT leads to adhesion failure as it lacks the capacity to effectively dissipate external forces. The rupture of hydrogen bonds and physical interactions within the hydrogel dissipates considerable energy, enhancing mechanical strength and toughness, and making it well-suited for strong adhesion, as seen on RINC surfaces. Cyclic lap-shear tests were conducted to evaluate the mechanical resilience and adhesion durability of HFLAT and HiRINC (Figure 2h,i and Figures S4 and S5, Supporting Information).[25] HFLAT failed after 80 cycles under a force of 8 kPa due to weak interfacial adhesion, while HiRINC sustained robust adhesion at over 40 kPa for >100 cycles, indicating superior resilience and resistance to stress.

We analyzed scanning electron microscopy (SEM) images at various stages–pre-hydrogel loading, post-hydrogel loading, and post-hydrogel peeling–across different hydrogel-impregnated substrates such as FLAT, RINC, silica thin films, and porous silica nanoparticle-coated surfaces (Figure S6, Supporting

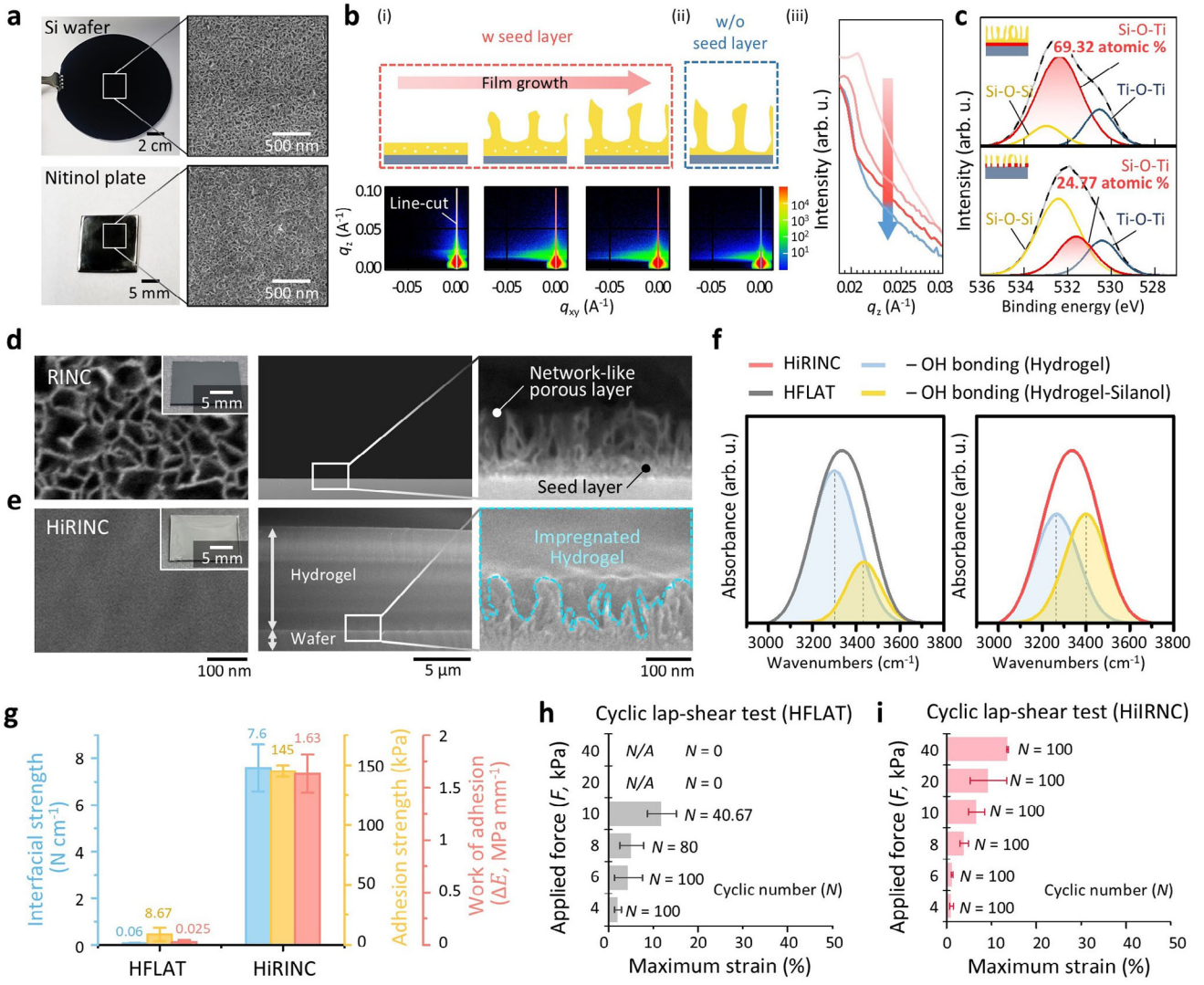

Figure 2. Bonding mechanism characterizations and strong adhesion property of hydrogel-impregnated robust interlocking nano connector (HiRINC). a) Photographs (left) and high-magnification (right) scanning electron microscopy (SEM) images of RINC on Si wafer and nitinol plate. b) Illustrations, grazing-incidence small-angle X-ray scattering (GISAXS) images, and line-cut profile of different RINC structures. c) XPS spectra showing the O 1s of the RINC on a nitinol substrate; with (top) and without (bottom) a seed layer. Optical images of top view (inset), SEM images of top view (left), low-magnification cross-sectional view (middle), and high-magnification cross-sectional view (right) of d) RINC and e) HiRINC. f) Deconvoluted Fourier transform infrared (FT-IR) spectra of the hydroxyl group for HFLAT (left) and HiRINC (right). g) Comparison of interfacial strength, adhesion strength, and work of adhesion values for HFLAT and HiRINC. h,i) Maximum strain and cyclic number (N) after a cyclic lap-shear test of a total of 100 cycles applied with various force values (F); HFLAT (h) and HiRINC (i). The data are presented as mean values ± standard deviation, representative of $n = 3$ independent experiments.

Information). Post peel tests, most of the porous silica nanoparticle-coated surfaces exhibited nanoparticle detachment, whereas RINC maintained its structural integrity even after the hydrogel was peeled off. The bonding energy between the substrate and RINC is higher compared to that between the hydrogel and RINC.[26] Although RINC had the same silica content as the other tested materials, its porous layer markedly increased the interfacial area for hydrogen bonding and promoted mechanical interlocking, thereby enhancing adhesion. These findings were corroborated by 90° peel tests using various commercial adhesive tapes (e.g., Kapton, masking, Scotch, and double-sided tapes), which revealed that the RINC exhibited greater interfacial strength (Figure S7, Supporting Information).

2.2. Durability of HiRINC Under Various Conditions

Figure 3a illustrates the cross-cut adhesion test used to evaluate hydrogel adhesion, showing the results for HFLAT and HiRINC in their as-prepared and swollen states, respectively. HFLAT exhibited extensive peeling of the hydrogel layer, indicating weak adhesion in its swollen state, which leads to delamination (Figure 3b,c). The hydrogel layer of HiRINC demonstrated

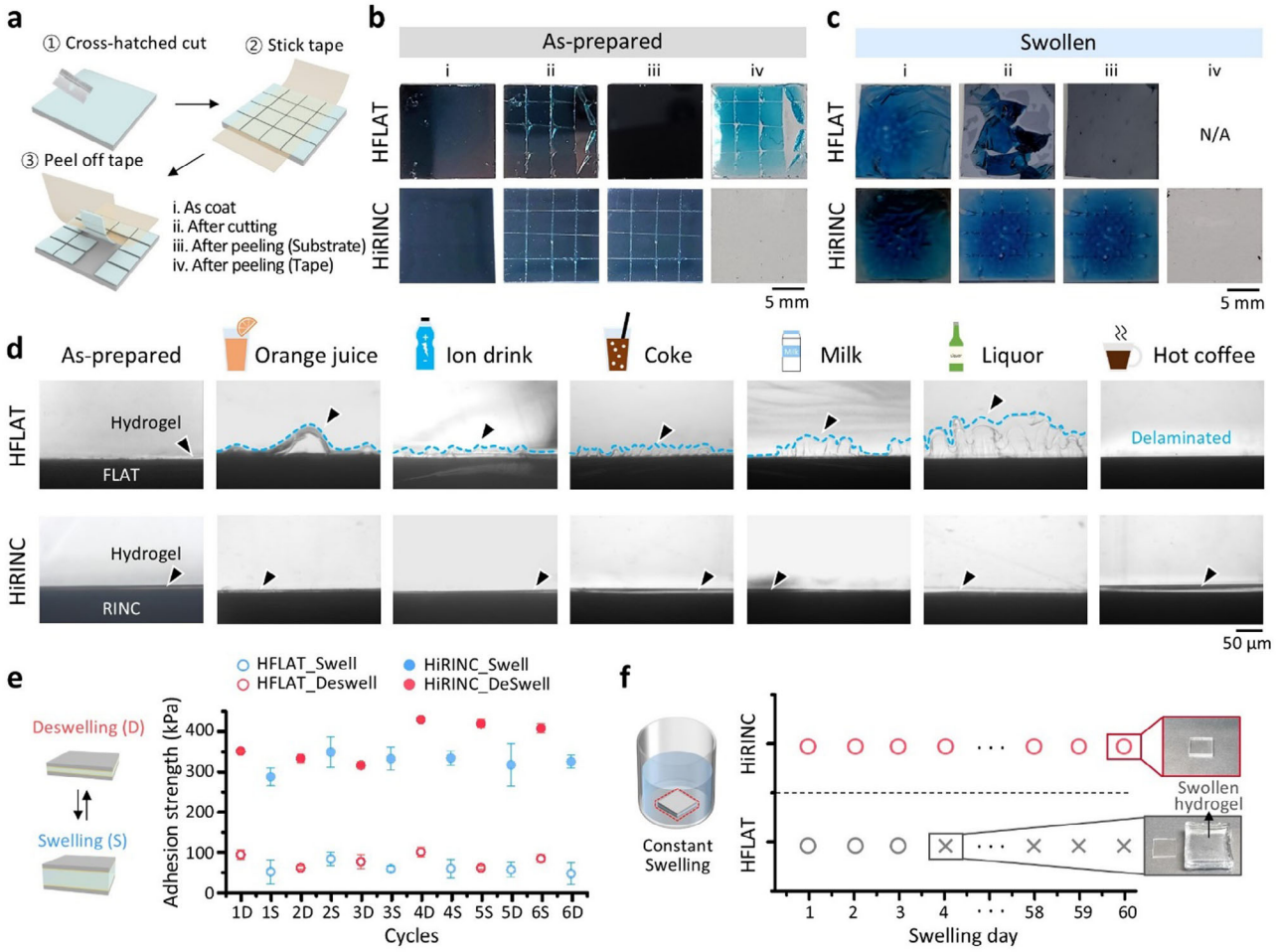

Figure 3. Swelling behavior and adhesion stability of hydrogel-impregnated robust interlocking nano connector (HiRINC) under different conditions. a) Schematic illustration of the process of a cross-cut test of the hydrogel layer. b,c) Photographs showing the differences in the morphology of the hydrogel layer for HFLAT and HiRINC at each step after cross-cut test at as-prepared state (b) and swelling state (c). d) Cross-sectional optical microscope images to compare swelling and adhesion behavior on HFLAT and HiRINC to observe swelling in different drinks for 1 h. e) Adhesion strength under cyclic deswelling-swelling for adhesion integrity assessment. The data are presented as mean values ± standard deviation, representative of $n = 3$ independent experiments. f) Graph showing adhesion or failure during swelling in water for 60 days. (Inset; Photographs of HiRINC (top) and HFLAT (bottom)).

superior adhesion during tape removal in both as-prepared and swollen states. The durability of the HFLAT and HiRINC surfaces when exposed to various liquids was compared (Figure 3d and Video S1, Supporting Information). The initial condition of each surface served as a reference, with black arrows indicating the hydrogel layers. The hydrogel of HFLAT changed its morphology (outlined by blue dashed lines) and delaminated upon exposure to hot coffee. This susceptibility to buckling and delamination was attributed to swelling-induced compressive stress, which causes instability, including wrinkles and buckles, exacerbated by the weak adhesion to the rigid substrate.[27] However, HiRINC exhibited no buckling or delamination, indicating that its strong adhesion was capable of withstanding exposure to various liquids, thereby ensuring stable performance.

Considering the frequent exposure of the esophagus to varying moisture levels from beverages and other substances, we conducted cyclic swelling-deswelling tests on HFLAT and HiRINC to evaluate their adhesive stability and durability. The adhesion of HiRINC was over three times stronger than that of HFLAT, even after multiple swelling and deswelling cycles (Figure 3e). Figure 3f illustrates the adhesion durability of both HiRINC and HFLAT in wet environments. Throughout the entire test period, HiRINC exhibited outstanding adhesion performance and maintained its structural integrity, whereas HFLAT completely delaminated by the fourth day, precluding further assessment. This pronounced disparity emphasizes the enhanced durability of HiRINC and its ability to withstand swelling-induced stress, while these factors undermined adhesive reliability of HFLAT (Figure S8, Supporting Information).

2.3. Ex Vivo Adhesive Performance of HiRINC and In Vivo Adhesive Performance of HiRINC-SEMS

Figure 4a and Video S2 (Supporting Information) provide photographic evidence from practical adhesion tests conducted on

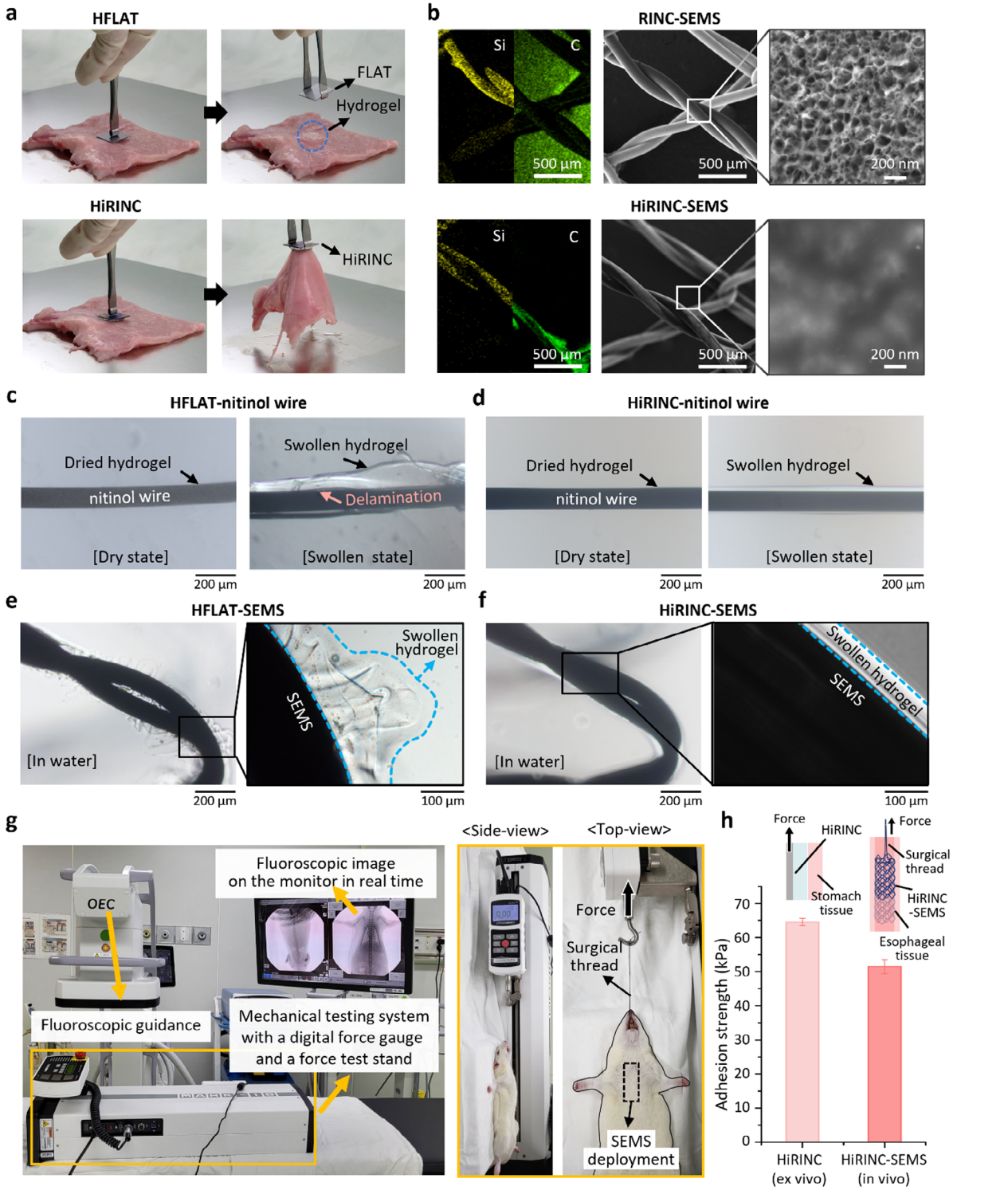

Figure 4. Hydrogel-impregnated robust interlocking nano connector-coated self-expandable metallic stent (HiRINC-SEMS) and in vivo adhesive performance. a) Photographs depicting the failure to lift up the porcine tissue due to the adhesion failure between hydrogel and FLAT (top) and photographs depicting successful lifting of the porcine tissue due to the strong adhesion between the tissue, and HiRINC (bottom). b) Energy-dispersive X-ray spectroscopy (EDS) mapping images (left), and scanning electron microscopy (SEM) images under low-magnification (middle) and high-magnification (right) of the RINC-coated self-expandable metallic stent (RINC-SEMS) (top) and the HiRINC-SEMS (bottom). c,d) Optical microscope images of the HFLAT (c) and the HiRINC (d) on the nitinol wire in dry (left) and swollen (right) state. e,f) Optical microscope images of the HFLAT-coated self-expandable metallic stent (HFLAT-SEMS) (e) and the HiRINC-SEMS (f) in swollen state at a low-magnification (left) and high-magnification (right). g) Experimental images depicting the integrated system of fluoroscopic imaging-integrated in vivo lap shear test. h) Comparison of adhesion strength of HiRINC in ex vivo and in vivo experiments. The data are presented as mean values ± standard deviation, representative of $n = 3$ independent experiments.

porcine stomach tissue (10 × 10 cm). The detachment of the hydrogel layer from the substrate (marked by a blue circle) indicates an immediate adhesion failure of HFLAT during lifting process. In contrast, HiRINC maintains robust adhesion under force, with the hydrogel remaining firmly attached to the substrate even when lifted from the tissue. We conducted quantitative adhesion strength tests on ex vivo porcine stomach tissue (1 × 1 cm). Figure S9 (Supporting Information) shows the superior tissue adhesive performance of HiRINC with an adhesion strength of 65 kPa, compared to the noticeably lower lap-shear strength of 5 kPa of HFLAT, indicating adhesion failure between the hydrogel and the flat surface. Polyvinyl alcohol and polyacrylic acid, being hydrophilic and hygroscopic, absorb interfacial water when in contact with wet tissues, thereby ensuring stability in wet and dynamic esophageal conditions. The carboxylic acid and NHS ester groups in the hydrogel interact with amino or carboxyl groups in mucosal cells, even with the diverse glycocalyx of epithelial surfaces,[28] resulting in strong and rapid adhesion through physical cross-linking via hydrogen bonds and covalent cross-linking via amide bonds. Cytotoxicity evaluation is essential for determining the potential use of these materials in medical devices.[29] The cytotoxicity of the control, HFLAT, and HiRINC was assessed by measuring the viability of AGS cells using the CCK-8 assay. Cell viability on all tested samples remained above 90% at all time points, indicating that none of the materials exhibited significant cytotoxicity (Figure S10a, Supporting Information).

Following the confirmation of the tissue-adhesive and noncytotoxic properties of HiRINC, we investigated its suitability as SEMS. Figure 4b shows the silicon distribution within RINC and carbon distribution within the hydrogel layer (Figure S11, Supporting Information). Figure 4c,d shows the contrasting behavior of the hydrogel layer on a nitinol wire. The HFLAT-nitinol wire swelled when immersed in water, after which delamination occurred due to inadequate adhesion. In contrast, the HiRINC-nitinol wire maintained the integrity of its hydrogel layer without delamination in both dry and swollen states. Furthermore, HFLAT-SEMS exhibited considerable hydrogel swelling, characterized by wrinkles, buckles, and delamination (indicated by dashed outlines in Figure 4e,f), suggesting instability when immersed in water. Conversely, the hydrogel of HiRINC-SEMS effectively adhered to the stent structure, including the curved areas, with minimal swelling observed. These unique behaviors of HFLAT-SEMS and HiRINC-SEMS in water emphasize the improved bonding and stability provided by the network-like porous layer.[30]

For real-time quantitative assessment of in vivo adhesion strength in the rat esophagus, we established a comprehensive test system, utilizing fluoroscopic guidance and a mechanical testing system equipped with a digital force gauge (Figure 4g). Before stent placement, a surgical thread was secured to the end of the stent. Subsequently, the HiRINC-SEMS was inserted into the middle portion of the rat esophagus under fluoroscopic guidance. After allowing approximately 1 min for the adequate adhesion to the esophagus, the protruding end of the thread from the mouth was connected to a force gauge, enabling the measurement of adhesion strength between the esophageal tissue and HiRINC-SEMS by pulling. The hydrogel layer remained intact after the in vivo lap shear test, indicating a robust and durable adhesion mechanism provided by the combination of hydrogel and RINC (Figure S12, Supporting Information). No esophageal tissue was observed on the stent surface after removal, indicating that HiRINC-SEMS did not cause detectable damage. Even if residual hydrogel remains on the esophageal tissue, its biocompatibility is expected to minimize inflammatory responses. The adhesion strength of HiRINC-SEMS measured in the in vivo lap shear test was slightly lower than that from the ex vivo test, but the values were still high (Figure 4h). Successful adhesion in the rat esophagus indicates its potential for clinical application.

2.4. In Vivo Anti-migration Properties and Histological Findings in a Rat Esophageal Model

All SEMSs were successfully placed in the rat esophagus without procedure-related complications (**Figure 5a**). However, one of the 18 (5.5%) rats in the HFLAT group experienced death 3 days after stent placement due to severe food impaction (Figure S13, Supporting Information). The remaining 17 (94.4%) rats survived until the end of the study (Figure 5b). The endoscopic findings revealed a blue-toned esophageal mucosa around the HFLAT- and HiRINC-SEMSs due to the activation of the hydrogel coating layers onto the surface of the SEMS (Figure S14, Supporting Information). All rats experienced transient weight loss immediately after stent placement, and their body weight started to recover after one week (Figure S15, Supporting Information). A significant difference in body weight change was observed among all groups after 4 weeks of stent placement ($p < 0.001$), with the HiRINC group showing the highest weight gain. All SEMS used in this study significantly influenced the incidence of migration ($p = 0.014$, Chi-squared test). Stent migration occurred in five of six rats (83.3%) in the control group within 7–14 days (mean, 10.5 days) after stent placement (Figures 5b,c and S16, Supporting Information). The remaining one rat was used for histological analysis. This high incidence, including both partial ($n = 2$) and complete ($n = 3$) migration, established the control group as a suitable animal model for investigating anti-migration stents. In the HFLAT group, partial migration occurred in two (40%) of five rats within 14–28 days (mean: 21 days). The incidence of stent migration in the control group was significantly higher than that in the HiRINC group ($p = 0.015$, Fisher's exact test) but did not differ with that of the HFLAT group ($p = 0.242$). There were no significant differences between the HFLAT and HiRINC ($p = 0.182$) groups. Stent patency in clinical practice should be maintained 3 to 6 months after stent placement according to the ranges of patient survival periods of unresectable malignant esophageal strictures.[4,31] Temporary stenting for patients with refractory benign esophageal stricture or patients with malignant stricture who underwent concurrent chemoradiation therapy was used from 4 to 6 weeks following the start of therapeutic plan.[32] Although we observed the presence of stent migration during 1-month follow-up period, stent migration mainly occurred in the early stage of stent placement. The placed stent becomes well fixed due to tissue growth though the stent meshes at 1-month onwards. The in vivo findings demonstrated the safety and efficacy of the stable HiRINC-SEMSs, which were fabricated using simple coating process, in the rat esophagus. As HiRINC-SEMS effectively prevented stent migration in the esophagus, which

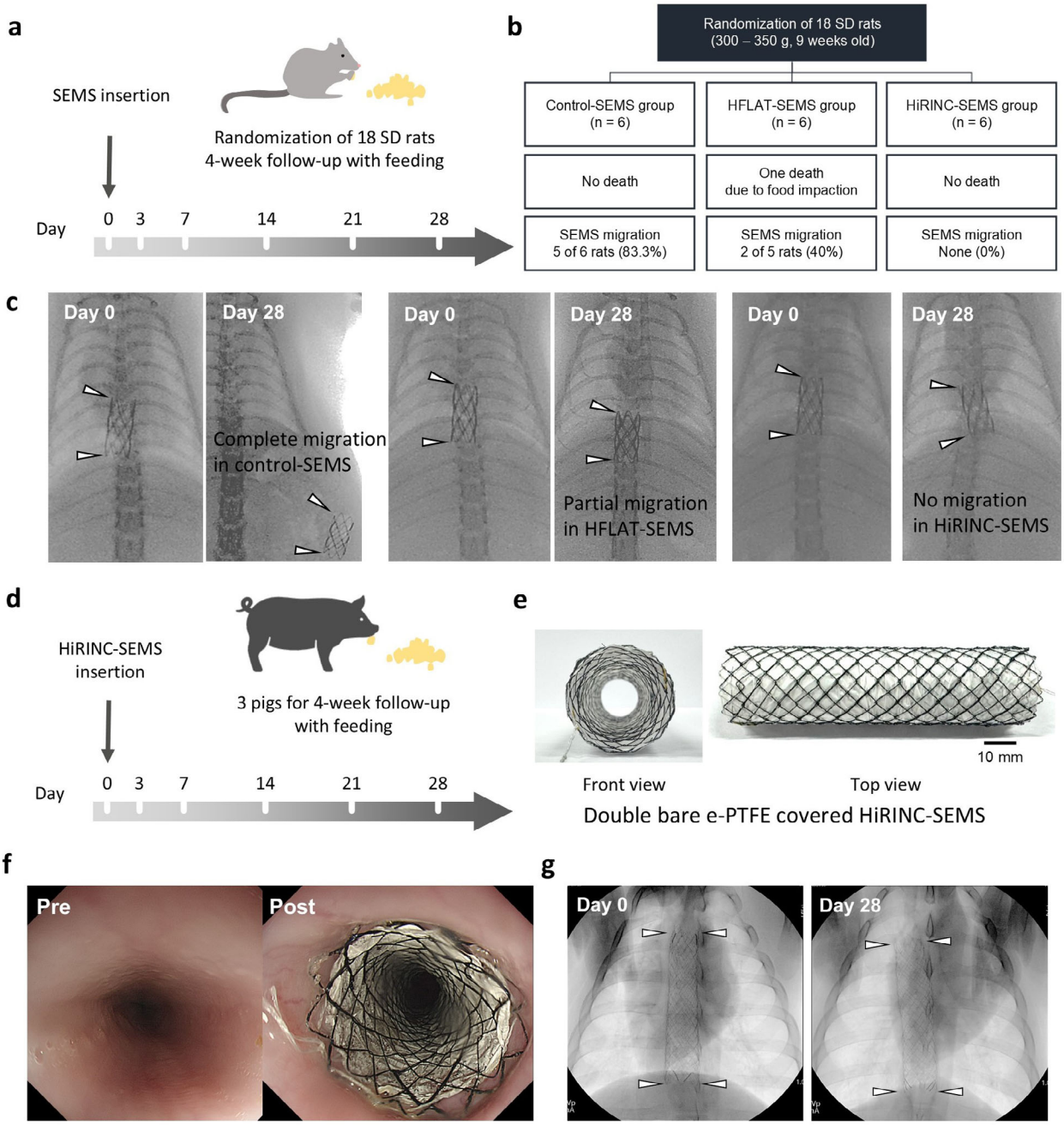

Figure 5. Results of in vivo experimental analysis. a) Experimental scheme in a rat esophageal model. b) Flowchart showing the randomization process and follow-up of rat in vivo study. c) Representative radiographic images obtained during the follow-up period showing the complete migration of the control self-expandable metallic stent (SEMS) into the stomach and the partial migration of HFLAT-SEMS to the distal portion of the lower esophagus, whereas the hydrogel-impregnated robust interlocking nano connector-coated SEMS (HiRINC-SEMS) maintains its position and shows no migration in the rat esophagus. d) Experimental scheme in a porcine esophageal model. e) Photographs showing the double bare expanded-polytetrafluoroethylene (e-PTFE) covered HiRINC-SEMS. f) Representative endoscopic images obtained before and immediately after placement of the double bare e-PTFE covered HiRINC-SEMS. g) Representative radiographic images showing the double bare e-PTFE covered HiRINC-SEMS well maintains its position without migration in the porcine esophagus.

shows active peristalsis, it can likely prevent migration in other luminal structures of similar or lower level of peristalsis, including the gastric outlet, duodenum, and colon.

The entire esophagus and stomach of all rats were successfully extracted. In the control group, SEMS migrated to the lower esophagus, as revealed by extracted esophageal samples (Figures S17 and S18, Supporting Information). Histological findings are summarized in Table S2 (Supporting Information) and shown in **Figures 6** and S19 (Supporting Information). The mean percentage of tissue hyperplasia area, thickness of

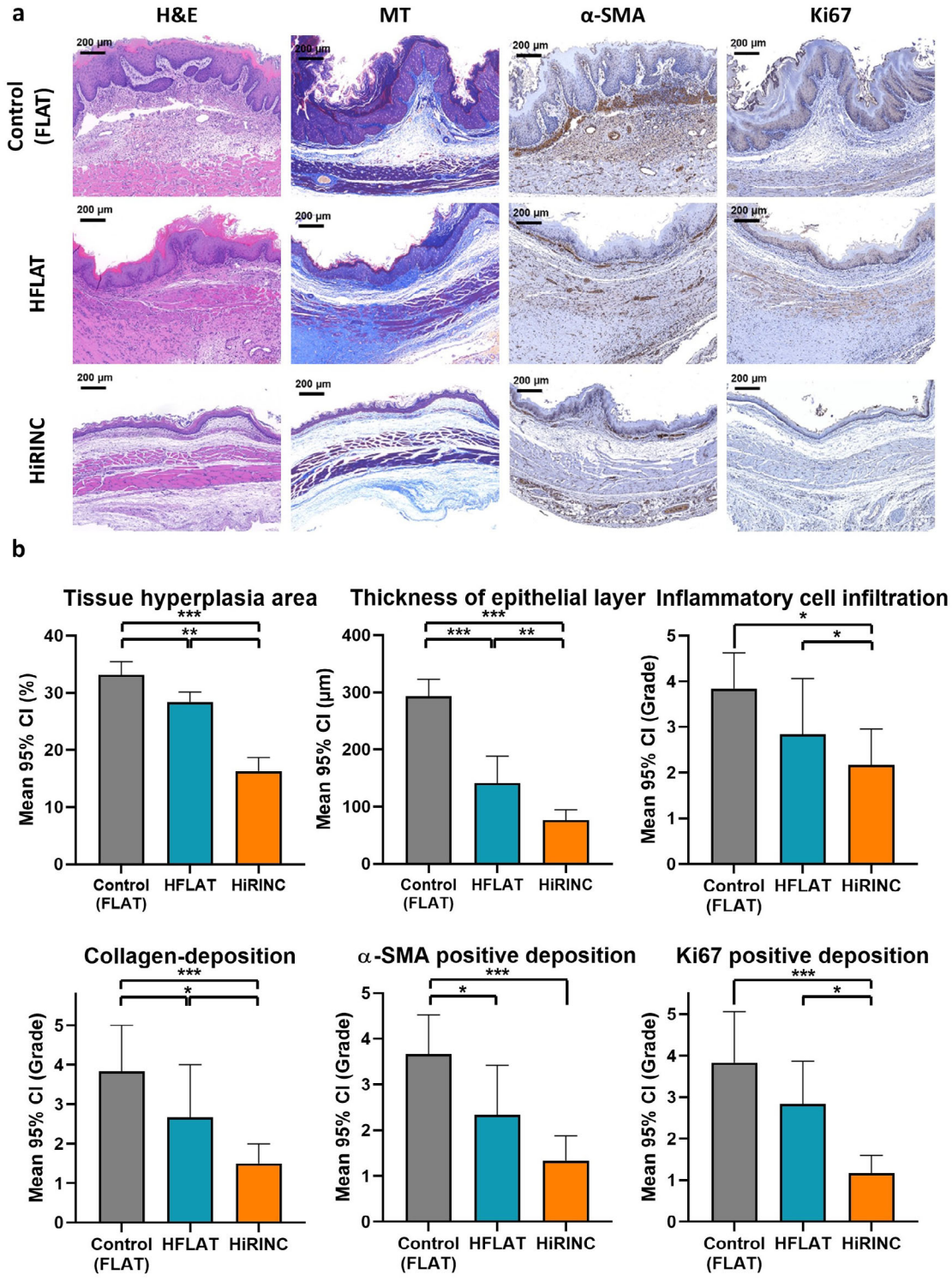

Figure 6. Histological findings after four weeks of self-expandable metallic stent (SEMS) placement in study groups. a) Representative microscopic images of histological sections showing the SEMS-induced tissue hyperplasia-related variables in the control group are significantly increased compared with those in the HFLAT and hydrogel-impregnated robust interlocking nano connector (HiRINC) groups. b) Histological analysis of the stented esophagus in the control, HFLAT, and HiRINC groups. The percentage of tissue hyperplasia area, thickness of the epithelial layer, mean degree of inflammatory cell infiltration, mean degree of collagen deposition, and mean degrees of α-SMA and Ki-67-positive deposition in the control group was significantly higher than those in the HFLAT and HiRINC groups. H&E, hematoxylin and eosin; MT, Masson's trichrome; α-SMA, α-smooth muscle actin marker; CI, confidence interval. The data are presented as mean values ± standard deviation ($n = 6$ per group) and one animal in the HFLAT group was excluded due to mortality. $^{*}p < 0.05$, $^{**}p < 0.01$, $^{***}p < 0.001$.

epithelial layer, degrees of inflammatory cell infiltration and collagen deposition, and degrees of α-SMA and Ki67-positive deposition were significantly different between the study groups (all variables; $p < 0.05$, one-way ANOVA). Stent-induced tissue hyperplasia related variables in the HFLAT and HiRINC groups were significantly decreased compared to the control group. HiRINC coating layers onto the surface of the SEMS can be attributed to the reduced inflammation in the stented tissue despite increased mechanical strength. The reduced inflammatory cell infiltration in the HFLAT and HiRINC groups could be attributed to the biocompatible nature of the hydrogel and RINC materials, which may minimize the foreign body reaction and subsequent inflammation.[33] Tissue healing resulting from mechanical injuries by stent can be divided into overlapping phases including inflammation, proliferation, and remodeling that occur over 4 weeks. The healing process immediately begins after stent-induced mechanical pressure and then the proliferative phase with increased fibroblasts and decreased inflammatory phase begins between 4 and 14 days.[34] The proportion of α-SMA, which indicates the presence of activated myofibroblasts, was decreased in the HiRINC group. Ki 67-positive deposition, which is a principal marker of cell proliferation, was also significantly lower in the HiRINC group than in the control and HFLAT groups. In particular, the HiRINC coating was more potent in preventing cell proliferation than the HFLAT coating. The HiRINC SEMS was effective and safe for inhibiting stent migration with decreased inflammatory reaction in the rat esophagus. Smooth muscle cells within the esophageal tissue play a crucial role in the process of SEMS migration.[35] Their contraction and relaxation, along with other factors such as peristalsis and esophageal motility, can influence the movement and positioning of the SEMS.[6a] The adhesive property of the hydrogel coated onto the SEMS surface on smooth muscle cells may contribute to the reduced incidence of SEMS migration in the HFLAT and HiRINC groups.[36] In addition to providing a strong attachment between the hydrogel and stent surface evidenced by the absence of hydrogel lamination, coating the stent with RINC prior to loading hydrogel further decreased the risk of stent-related complications at the microscopic level. Hence, using RINC likely enhanced the stability of the hydrogel layer in the long run and maintained the stent position for long period.

2.5. Efficacy and Safety of Double Bare ePTFE-Covered HiRINC-SEMSs in the Porcine Esophagus

The double bare expanded-polytetrafluoroethylene (e-PTFE) covered HiRINC-SEMS, similar to those used in clinical practice, were successfully fabricated. A straight SEMS was designed with an e-PTFE membrane attached between two bare SEMSs to facilitate stent migration and to reduce pain and foreign body reaction. HiRINC was coated onto the surface of the external bare SEMS to prevent migration (Figure 5e). To evaluate the potential of translating the SEMS in a clinical setting, the double bare e-PTFE covered SEMS was placed into the porcine esophagus in a minimally invasive manner with a follow-up period of 4 weeks (Figure 5d). The double bare e-PTFE covered HiRINC-SEMS was successfully placed at the level of the mid-costal cartilage of the esophagus without procedure-related complications. Follow-up radiographic images demonstrated that stent migration did not occur during the follow-up period in all pigs (Figure 5g). On gross examination, esophageal tissue injuries were not observed immediately after stent removal. Histological findings are presented in Table S3 and Figure S20, Supporting Information. In the HiRINC group, an enlarged luminal area compared to the normal esophageal tissue (79.08 ± 3.18 versus 32.46 ± 3.59 mm^2, $p < 0.001$) was observed, which was caused by mechanical pressure of the SEMS. The degrees of inflammatory cell infiltration ($p = 0.104$) and collagen deposition ($p = 0.355$) did not differ between the stented and normal esophagus, but slightly increased in the HiRINC group. These findings were corroborated by in vivo results of the rat esophageal model as HiRINC-SEMS demonstrated lower levels of inflammation compared to control SEMS. The consistency of these results across both rat and porcine models suggested that the biocompatible nature of the hydrogel and RINC materials may effectively mitigate the inflammatory response typically associated with stent placement, regardless of the animal species. Furthermore, the HiRINC-SEMS not only maintained its position without migration but also potentially contributed to preserving luminal patency while minimizing the stent-induced tissue hyperplasia resulting from reduced inflammatory response. HiRINC-SEMS demonstrated potential to address key limitations of conventional stents including migration, stent patency, and excessive inflammatory response. These improvements suggested that HiRINC-SEMS may enhance clinical outcomes for patients requiring esophageal stenting. Our findings suggest that our strategy can be translated into a clinical setting and can be extended to other endoluminal organs where SEMSs are commonly used. Placement of the double bare e-PTFE covered HiRINC-SEMS was effective and safe to prevent stent migration with reduced inflammatory reaction in a porcine esophageal model. Our anti-migration strategy using surface modification of SEMS significantly reduced stent migration rates via enhancing the adhesive force between the SEMS and esophageal tissue without additional procedures while maintaining conventional procedural steps. HiRINC, made of biocompatible materials, can be easily applied to the uncovered or covered SEMS.

3. Conclusion

SEMS placement is a standard therapeutic option for dysphagia resulting from malignant and benign esophageal stricture in clinical settings; however, stent migration limits successful stent placement. Our study addressed this challenge by exploring the efficacy of RINC structure in enhancing stent adhesion and stability within the dynamic environment of the esophagus. HiRINC-SEMS outperformed control SEMS in preventing migration, primarily due to the increased surface area and mechanical interlocking features of the nanostructured RINC design, which enhance adhesion strength and durability.[16c] This reduces the structural mismatch between stents and esophageal tissues, thereby reducing migration risks.

We also examined specific design parameters of RINC structure, including pore size and film thickness, to assess their effects on adhesion. Small pores (1–2 nm), which were smaller than those in HiRINC, hindered hydrogel penetration, whereas large pores (>100 nm) reduced mechanical interlocking, thereby

diminishing the adhesion strength (Figure S21, Supporting Information). Further, the films thinner than those used in HiRINC decreased adhesion due to insufficient interlocking, whereas thicker films initially enhanced adhesion strength and then attained a threshold, beyond which no further improvement was observed. This was likely due to pore filling, indicating the importance of balancing these variables to maximize adhesion performance. Our findings also highlight the importance of addressing potential complications associated with hydrogel swelling, which can lead to severe esophageal blockages. The anti-swelling properties of HiRINC could effectively mitigate this risk, ensuring that the hydrogel does not expand to a degree that compromises the esophageal lumen. This understanding can help maintain the benefits of hydrogel coating while minimizing associated risks.

In-stent restenosis, caused by tissue growth and stent migration are major obstacles to successful stent placement in nonvascular luminal organs. SEMS placement in a rat esophageal model is well-established animal model with high technical success and survival rates. We selected SEMS diameter as 5 mm, based on a previous study that indicated a migration rate (40%) similar to the clinically reported rate (approximately 33%).[37] We adopted several experimental measures to promote SEMS migration. While most previous studies typically used SEMS of length 12–15 mm in rat esophagus, we selected a shorter length of 10 mm, which is more conducive to migration.[19a,34c,37,38] Further, barbs are typically attached to the middle portion of the SEMS to prevent migration in a rat esophageal model; however, the barbs were omitted in our study to enhance migration rate.[19a,37,38] Additionally, while the proximal end of the SEMS is typically placed in the upper esophagus of the clavicle level under fluoroscopic guidance to prevent migration, we placed the distal end at the diaphragm level to encourage migration.[19a,34c,38] The incidence of SEMS migration was very high in the control group (83.3%) making it a suitable model for investigating anti-migration SEMSs.

Our study provides valuable insights into HiRINC-SEMS, but it had a few limitations. Our experimental conditions may not fully capture the potential fragility of HiRINC-SEMS in real-world scenarios where ongoing physical activity and varying bodily conditions could impact the durability of the stent. Additionally, as the SEMS were only tested in normal rat esophagi, tissue response in pathological conditions such as esophageal strictures and other human pathological mechanisms may differ. Our results attained statistical significance, but the small sample size may limit the robustness of our statistical analysis. However, according to the "resource equation" method, an E value of 15 is effective and meets the ethical standards for animal experimentation. Additionally, the long-term effectiveness of the HiRINC-SEMS was not evaluated. Lastly, the remaining amount of hydrogel on the SEMS and the degree of hydrogel delamination were not evaluated during the last follow-up. Further research is required to confirm and optimize our findings. Nonetheless, this preliminary study provides a strong foundation for the advanced development of anti-migration stents. HiRINC-SEMS demonstrates significant potential as an innovative platform for preventing stent migration, applicable not only in the esophagus but potentially in nonvascular luminal organs, paving the way for potential improvements in clinical management and treatment strategies.

4. Experimental Section

Synthesis and Physical Stability Test of Robust-Interlocking Nano Connector (RINC): Substrates (Si wafers, nitinol plates, glass, and nitinol SEMS) were washed by sonication using acetone, ethanol, and deionized water; dried in an oven; and treated with O_2 plasma (CUTE, FEMTO Science) at a flow rate of 30 sccm under a power of 100 W for 40 s, immediately before fabricating RINC. RINC containing a seed layer was fabricated by dissolving 19×10^{-3} M triethanolamine (TEA, ≥99.0%, Sigma-Aldrich) in deionized water at 80 °C with vigorous stirring, followed by the introduction of the substrates. To this solution, 75×10^{-3} M sodium salicylate (NaSal, ≥99.5%, Sigma-Aldrich) and 0.69 M cetyltrimethylammonium chloride (CTAC, 25 wt% in H_2O, Sigma-Aldrich) were added. After 1 h of stirring for stabilization and substrate fixation of micelles, 4.5 M of tetraethyl orthosilicate (TEOS, 98%, Sigma-Aldrich) was added gradually (dropwise) as a silica precursor. The mixture was stirred for 1–2 h, and the obtained RINC-coated substrates were sonicated several times with ethanol and distilled water to eliminate the residual reactants.

RINC without seed layer was fabricated similarly except that the substrate was introduced after micelle stabilization. After RINC synthesis, the physical stability of the seed layer was compared using a homogenizer (KUS-650, KBT) with 600 W of power for 2 min in a 70% (w/w) ethanol solution. Pore size and film thickness of RINC were controlled by changing the reagents and the TEOS reaction time. Small pores could be synthesized using only CTAC for micelle formation, and large pores could be synthesized without TEA.[1] The longer the reaction time of TEOS, the thicker film was obtained.

Fabrication of Hydrogel-Coated FLAT (HFLAT) and Hydrogel-Impregnated RINC (HiRINC): The hydrogel precursor was prepared by mixing 700 mg PVA (M_w = 146 000 to 186 000, ≥99% hydrolyzed, Sigma-Aldrich) in 6.6 mL deionized water at 90 °C, with a sequential addition of 3.3 mL acrylic acid (99%, Sigma-Aldrich), 20 mg α-ketoglutaric acid (99.0 to 101.0%, Sigma-Aldrich), 4.55 µL poly(ethylene glycol) dimethacrylate (M_n = 550, Sigma-Aldrich), and 30 mg acrylic acid N-hydroxysuccinimide ester (≥90%, Sigma-Aldrich). Finally, the hydrogel precursor was stirred thoroughly and stored away from ultraviolet (UV) light.

Hydrogel coated samples were produced by mold coating or dip coating based on the experiment. Mold coating involved placing the polydimethylsiloxane mold on the substrate and pouring the hydrogel precursor to obtain a desired dimension of hydrogel coating. Dip coating was performed by retrieving the substrate at a rate of 13 mm min^{-1} from the hydrogel precursor. After hydrogel coating, samples were cured using a UV lamp (365 nm, 15 W power) for a certain time to fabricate HFLAT and HiRINC.

Real Area Measurement: The real area of RINC was measured by capacitance method. The real area was determined using the following equation: C_{dl}/C_S, where C_{dl} is the double-layer capacitance and C_S is the specific capacitance of Si wafer with a geometric surface area of 1.0 cm^2. The C_{dl} was measured by cyclic voltammetry in the non-Faraday region. To estimate C_{dl}, $\Delta j = |j_a - j_c|$ at 0.05 V (versus Ag/AgCl) was plotted as a function of different scan rates, where j_a and j_c are the anodic and cathodic current densities, respectively. The measurements were conducted in a 0.1 M perchloric acid ($HClO_4$) solution saturated with N_2 gas.

Adhesion Measurements: Adhesion properties were measured by obtaining force–displacement curves using a mechanical testing system equipped with a digital force gauge (ESM303, Mark-10) and force test stand (F305-EM, Mark-10). For 90° peel test, HFLAT and HiRINC samples were fabricated using mold-coating process. To prevent hydrogel deformation during the test, a rigid backing of polyethylene terephthalate film was bonded with cyanoacrylate glue gel (Loctite 401 Flex Gel, 3M) after the hydrogel coating. For 90° adhesion test, commercial tapes (Kapton tape, masking tape, 3M Scotch tape, and 3 M double-sided tape) were applied on the testing surfaces and pressed with a constant force and time before the measurement. To measure interfacial strength, an adhesion area of 10×30 mm^2 was created, and a 90° peel test was conducted at a fixed rate of 13 mm min^{-1}. The average force value was calculated from the curve obtained between displacement range of 10–20 mm.

Lap shear test was conducted using a testing sample prepared by mold-coating hydrogel between two substrates. Slide glasses were attached to

the testing sample as a backing fixture to fix the sample to the clamp of the testing instrument. Adhesion strength was determined by calculating the maximum value at the lap shear load-displacement curve, and energy dissipation was obtained by integrating the area under the curve. To assess the interfacial fatigue threshold, a cyclic lap shear test was conducted using force control mode. A constant force (F) ranging from 4 to 40 kPa was applied to the test samples for N cycles (maximum 100 cycles). The maximum strain is defined as the ratio of the distance measured at the point where F was last reached to the adhesion length. The lap shear test was conducted at a rate of 50 mm min^{-1} for an adhesion area of 10×10 mm^2.

Preparation of Various Silica Surfaces: The precursor for the silica thin film was prepared as follows: 100 µL acetic acid (≥99.7%, Sigma-Aldrich) was added to 840 µL of anhydrous ethanol, followed by stirring. Thereafter, 60 µL TEOS was added, and when the mixture was sufficiently blended, 100 µL distilled water was added dropwise and mixed for 1 h. To fabricate a thin film, the precursor was dispensed on the substrate, followed by spin coating at 9000 rpm for 10 s and baking at 200 °C for 1 h.

Porous silica nanoparticles were obtained from the reaction solution after RINC synthesis, and the dispersed solution containing porous silica nanoparticles was dispensed onto the substrate and spin-coated at 9000 rpm for 10 s.

To functionalize the amine groups, O_2 plasma-treated substrates were immersed in 5% (v/v) 3-aminopropyltriethoxysilane solution (99%, Sigma-Aldrich) (in 100 mL toluene) added with 200 µL Triton-X (Sigma-Aldrich). The functionalization process was carried out under an argon atmosphere with constant stirring at 50 °C for 3 h. After functionalization, the surface was washed with anhydrous ethanol for 10 min and dried in N_2 gas.

Cross-Cut Test: The adhesive strength of dip-coated hydrogel on FLAT and RINC, each with a size of 15×15 mm^2, was evaluated by creating crosshatch cuts using blades. To obtain swelling conditions, hydrogel-coated substrates were immersed in deionized water for 1 h. Finally, tape (Scotch tape, 3 M) was applied to the scratched samples using a constant force and then removed by peeling 180°.

Microscopic Imaging of Hydrogel-Coated Substrates: The samples for microscopic imaging were prepared by dip-coating hydrogel onto the substrates. The hydrogel coatings were observed using microscopic videos (IX73, Olympus) at 40× and 200× magnification, starting from the dry state and continuing for 1 h to monitor the swelling process. To monitor the swelling of HFLAT and HiRINC in cross-sectional view, the test samples were cross-cut and attached to a fixture before exposure to various liquids for allowing them to swell (water, orange juice, ion drink, coke, milk, liquor, and hot coffee).

Adhesion Characteristics Under Alternating Swelling-Deswelling and Constant Swelling Conditions: Hydrogel coating was applied in a sandwich style between two substrates to measure adhesion properties under different swelling environments. The cyclic swelling-deswelling process consisted of alternating steps. First, the samples were soaked in deionized water for 30 min during the swelling step, followed by drying at 70 °C for deswelling step. Adhesion tests were conducted after each step. To compare the detachment of hydrogel between HFLAT and HiRINC under swelling conditions, the samples underwent swelling in deionized water for up to 60 days.

Anti-Swelling Test: The hydrogel was molded into a cylindrical form with a diameter of 10 mm and a height of 0.5 mm. The swelling performance was tested by immersing the hydrogel samples in deionized water at room temperature. The weight, diameter, and thickness were measured at a certain swelling interval and the swelling ratio was defined as the increase in these measured values compared to the initial state of the samples.

Adhesion Measurement on Ex Vivo Porcine Stomach Tissue: FLAT or RINC was applied on one side of hydrogel coating to allow for the attachment of porcine stomach tissue on the opposite side of the hydrogel. The porcine stomach tissue (10×10 cm) was immersed in a saline solution for washing, following which any remaining saline residue was wiped off from the stomach tissue. To demonstrate tough adhesion between hydrogel and porcine stomach tissue, the hydrogel side of the HFLAT and HiRINC were then applied to the tissue by gently pressing for 30 s. Thereafter, the adhesion strength was measured by employing lap shear test with a rate of 50 mm min^{-1}. Cyanoacrylate glue gel (Loctite 401 Flex Gel, 3 M) was utilized to fix the integrated testing safmples to the slide glass backing fixture and attach to the clamp of the lap shear testing instrument.

In Vitro Cell Cytotoxicity: The in vitro cell cytotoxicity of the FLAT, HFLAT, RINC, and Hiryn layers was investigated. Briefly, AGS (American Type Culture Collection, Rockville, MD, USA) cell line was cultivated in RPMI1640 (R8758; Sigma Aldrich, St. Louis, MO, USA) supplemented with 10% fetal bovine serum (SH30919.03; GE Healthcare Life Sciences, Logan, UT, USA) and 1% penicillin-streptomycin (17-745E; Lonza Bioscience, Walkersville, MD, USA), at 37 °C and 5% CO_2. The confluent cells (70%-85%) were washed, trypsinized using trypsin-EDTA 0.25% (Life Technologies, Gaithersburg, MD, USA), and re-seeded into 12-well plates for cytotoxicity test. The cell viability on the nanostructured substrate (1×1 cm^2) was determined using a Cell Counting Kit-8 assay (CCK-8; DOJINDO, Kumamoto, Japan). Each substrate was placed on a 12-well plate, and AGS cells were seeded at a concentration of 5×10^5 cells per well. The cells were then cultured at 37 °C, 5% CO_2 incubator. The cultures were then divided into three groups and incubated for different time periods (12, 24, and 48 h, respectively) before being assessed. After incubation, the medium was removed, the CCK-8 solution was added, and plates were incubated with the cells attached to the substrate for another 1 h. The absorbance of the supernatant was measured using microplate reader (Synergy HTX; BioTek, Winooski, VT, USA) at 450 nm. Live/Dead assay was performed according to the manufacturer's protocol. Live and dead cells were stained with Calcein AM and EthD-1, respectively. Fluorescence images of the cells were obtained using a fluorescence microscope (EVOS FL Auto, Life Technologies, Carlsbad, USA), and ImageJ software was used to analyze the fluorescence imaging results. All experiments were repeated three times, and the results were averaged.

Characterizations: Surface morphology was characterized using a Zeiss Sigma 300 field-emission scanning electron microscope (FE-SEM) operated at 1.5 kV (Center for Polymers and Composite Materials, Hanyang University, Korea). Elemental mappings were acquired by conducting energy-dispersive X-ray spectroscopy (EDS) using the same FE-SEM at 15 kV. GISAXS measurements were made using Xeuss 3.0 (Kyungpook National University, Korea.). The X-ray source was Cu Kα (8 keV), and the sample-to-detector distance and incident angle were 1000 mm and 0.05°, respectively. The confirmation of functional groups in HFLAT and HiRINC was conducted from 2900 to 3800 cm^{-1} using FT-IR under the attenuated total internal reflection mode (iS50, Thermo Fisher Scientific) at the Center for Polymers and Composite Materials, Hanyang University, Korea. The chemical composition of the surface was analyzed using a Thetaprobe X-ray photoelectron spectrometer (Thermo Fisher Scientific Co., Waltham, MA, USA) equipped with a scanning monochromated Al Kα source (Spot size; 400 µm). The X-ray beam collected information on the O 1s element for Figure 1c and C 1s and O 1s, and Si 2p elements for depth profiling (Figure S2, Supporting Information). The etching of depth profiling was performed using an Ar ion source (operated at 2 kV, 2 µA), with a time interval of 67 s between each step.

In Vivo Lap Shear Test Setup and Adhesion Measurement in a Rat Esophageal Model: For in vivo lap shear test in the rat model, mechanical testing system was installed on a radiographic table and then integrated with the fluoroscopic guidance. HiRINC-SEMSs were tied using a medical suture thread, and SEMS was introduced into the rat esophagus using a pusher catheter. Thereafter, rats were fixed in a supine position under the fluoroscopic guidance. The end of the thread was horizontally hung to the force gauge using the mechanical testing system to ensure precise lap shear strength measurement, followed by the initiation of the in vivo lap shear test at a rate of 50 mm min^{-1}. Accordingly, the utilized SEMSs were retrieved, and residual hydrogel coating images were observed with scanning electron microscope. To calculate the adhesion strength, the surface area was measured from an optical image of SEMSs using ImageJ software.

Anti-Migration Properties In Vivo Rat Esophageal Model: The in vivo rat animal study used in this study was approved by the Institutional Animal Care and Use Committee of the Asan Institute for Life Sciences

(2022-12-159) and conformed to the Guide for the Care and Use of Laboratory Animals. For the rat esophagus, the SEMS (S&G biotech Co., Ltd., Yongin, Korea) was hand-woven using a single thread of 0.127 mm-thick nitinol wire. The stents were 5 mm in diameter and 10 mm in length when fully expanded. The stent delivery system consisted of a 6 Fr Teflon sheath (Cook, Bloomington, IN, USA) and a pusher catheter. A total of 27 Sprague–Dawley rats (300–350 g, 9 weeks old; Orient Bio, Seongnam, Korea) were used for Figure 5a–c. The rats were randomly divided into three groups with nine rats in each: control group, HFLAT group, and HiRINC group; the rats in the three groups underwent implantation with control SEMS, HFLAT-SEMS, and HiRINC SEMS, respectively. The three rats in each group were sacrificed at 1 week after stent placement to evaluate inflammatory reaction in the early stage. The remaining six rats in each group were sacrificed at 4 weeks after stent placement to evaluate the incidence of stent migration and late tissue response. Sample size was determined using the "resource equation":

$$E\text{−value} = \text{total number of animals} - \text{total number of groups} \quad (1)$$

where, E is the degree of freedom of analysis of variance with values between 10 and 20.[2] All animals were housed under a 12-h light/dark cycle at environmental temperature (24 ± 1 °C) and humidity (55 ± 10%) with free access to food and water. The detailed technical steps of stent placement in the rat esophagus have been previously described.[3] Before the procedure, all rats were routinely anesthetized by intramuscularly injecting 50 mg kg^{-1} zolazepam and tiletamine (Zoletil 50; Virbac, Carros, France) and 10 mg kg^{-1} xylazine (Rompun; Bayer Healthcare, Leverkusen, Germany) and placed in a supine position. Each stent was loaded into a customized 6-Fr sheath with a pusher catheter, and this sheath was carefully advanced through the body of the rat into the esophagus. The stent was deployed under fluoroscopic guidance (OEC Elite CFD, GE Healthcare, Boston, MA, USA) at the level of the mid-costal cartilage of the esophagus, with the distal end of the stent positioned at the diaphragm level. Radiograph was obtained immediately after stent placement to record stent location in all rats. Radiographic follow-up examinations were performed at day 3 and weeks 1, 2, 3, and 4 after stent placement to check any changes in the stent location. All rats were euthanized by exposure to pure carbon dioxide after 4 weeks of stent placement.

Efficacy and Safety of HiRINC-SEMS in a Porcine Esophageal Model: The animal study was conducted in accordance with the Institutional Animal Care and Use Committee of the Asan Institute for Life Sciences (2024-20-113) and conformed to the Guide for the Care and Use of Laboratory Animals. The SEMS placed in the porcine esophagus had a double-bare structure comprising an outer and inner SEMSs. An e-PTFE membrane was attached between the outer and inner SEMSs to prevent tissue growth through the wire meshes. The SEMS was 24 mm in diameter and 120 mm length, and both of its ends were straight. HiRINC coating was only performed onto the surface of the outer SEMS. The stent delivery system consisted of a 24 Fr Teflon sheath and a pusher catheter. Three male juvenile pigs (International Animal Experiment Center, Pocheon, Korea) weighing approximately 20–30 kg were obtained and subjected to an acclimation period of 7 days before the procedure. The double bare e-PTFE covered HiRINC-SEMS was placed at the level of the mid-costal cartilage of the esophagus, whereas the remaining normal esophageal tissue adjacent to the stented area served as an internal control. After 24 h of fasting and under the supervision of a veterinarian, all pigs were placed under respiratory anesthesia after intramuscular injection of a mixture of 50 mg kg^{-1} zolazepam, 50 mg kg^{-1} tiletamine (Zoletil 50; Virbac, Carros, France), and 10 mg kg^{-1} xylazine (Rompun; Bayer Healthcare, Leverkusen, Germany). An endotracheal tube was placed, and anesthesia was administered by exposure to 1:1 mixture of 0.5%–2% isoflurane (Ifran; Hana Pharm. Co., Seoul, Korea) and oxygen (510 mL kg^{-1} min^{-1}). All procedures were performed in the left decubitus position. Pre-procedural endoscope examination (CF-H260AI; Olympus Inc. Tokyo, Japan) was performed, and an overtube was inserted through the mouth into the esophagus. Thereafter, a 0.035-inch guidewire (Radifocus M; Terumo, Tokyo, Japan) was passed through the overtube into the esophagus, which was followed by advancing the stent delivery system over the guidewire into the esophagus under fluoroscopic guidance. The pusher catheter was held in place, while the sheath was slowly withdrawn under continuous monitoring (Figure S22, Supporting Information). Post-procedural endoscopic examination was performed, and radiographic image was obtained immediately after stent placement to check its position (Figure 5f). Antibiotics (gentamicin, 7 mg kg^{-1}; Shin Poong Pharm Ltd., Seoul, Korea) and analgesics (keromin, ketorolac 1 mg kg^{-1}; Hana Pharm Ltd., Seoul, Korea) were administered for 3 days after the procedures. Radiographic images were obtained at day 3, 7, 14, and 28 after stent placement to monitor stent position and stent-related adverse events. After the follow-up studies, all pigs were immediately euthanized by injecting 75 mg kg^{-1} potassium chloride (KCl; Dai Han Pharm CO., Seoul, Korea) via the marginal ear vein.

Follow-Up Study and Definition of Stent Migration: Body weight and behavior changes were observed and recorded weekly in all animals. If stent migration was detected during the follow-up periods, euthanasia was induced immediately to review the results from the gross examination. Stent migration was defined as the movement of a placed SEMS above or below its proper positions, as revealed by radiologic findings. Stent migration was classified as partial if the stent migrated partially in the distal or proximal direction or complete migration if the stent migrated completely into the stomach or small bowel.

Histological Examination: The esophagus and stomach were harvested for subsequent analyses. After gross examination to determine possible esophageal injury, the stented esophagus was fixed in 10% neutral buffered formalin for 24 h, following which it was transversely sectioned at the proximal, middle, and distal regions. The stented porcine esophagus was analyzed by dividing them into three segments: normal, proximal, and distal portions of the stented esophagus. All specimens were embedded in paraffin, and sectioned to 4-µm-thick slices for histological and/or immunohistochemical (IHC) evaluation of changes in stented esophageal tissues. The slides were stained with hematoxylin and eosin (H&E) and Masson's trichrome (MT). H&E staining determined the mean thickness of the epithelial layer and the mean degree of inflammatory cell infiltration; the percentage of tissue hyperplasia area was calculated as 100 × (1 − [stenotic stented area/original stented area]).[3,4] The degree of collagen deposition was graded on MT-stained sections. The degrees of inflammatory cell infiltration and collagen deposition were subjectively determined according to the distribution and density of the cells and graded as 1–5 for mild, mild to moderate, moderate, moderate to severe, and severe, respectively. The analysis was performed using a digital slide scanner (Pannoramic 250 FLASH III, 3D HISTECH Ltd., Budapest, Hungary), and measurements were obtained with a digital microscope viewer (CaseViewer, 3D HISTECH Ltd.). The analyses of histological findings were based on the consensus of three observers blinded to the grouping. IHC analysis was performed on paraffin-embedded sections with α-smooth muscle actin (α-SMA, 1:200; Abcam, Cambridge, UK) and Ki-67 (1:250; Abcam) as the primary antibodies. After counterstaining with H&E, the sections were visualized using BenchMark XT, which is an automated IHC stainer (Ventana Medical Systems, Tucson, AZ, USA). The degrees of α-SMA– and Ki-67–positive depositions were subjectively determined according to the distribution and density of the cells and graded as 1–5 for mild, mild to moderate, moderate, moderate to severe, and severe, respectively. IHC findings were obtained based on the consensus of three observers blinded to the grouping.

Statistical Analysis: Data are expressed as mean ± standard deviation. ANOVA with Tukey post hoc test was performed for comparing multiple groups. Independent two-tailed Student's t-test was employed to determine the differences between two groups in some cases. p-values < 0.05 were considered statistically significant. Statistical analyses were performed using SPSS software (version 27.0; SPSS, IBM, Chicago, IL, USA).

Animal Ethics Statement: All animal experiments were conducted in accordance with the protocols approved by the Institutional Animal Care and Use Committee of the Asan Institute for Life Sciences (approval numbers: 2022-12-159 and 2024-20-113) and conformed to the Guide for the Care and Use of Laboratory Animals. Sprague–Dawley rats (300–350 g, 9 weeks old) were purchased from Orient Bio (Seongnam, Korea). Male juvenile pigs (20–30 kg) were obtained from International Animal

Experiment Center (Pocheon, Korea) and underwent a 7-day acclimation period before experimentation. All animals were housed under controlled conditions with free access to food and water throughout the experimental period.

Supporting Information

Supporting Information is available from the Wiley Online Library or from the author.

Acknowledgements

E.J., S.H.K., and S.K. contributed equally to this work. This work was supported by the National Research Foundation of Korea (NRF) grant funded by the Korean government (MSIT) (2023R1A2C2003128, 2022R1C1C1003205, 2022M3H4A1A04073271). This work was also supported by a grant (2025IP0009) from the Asan Institute for Life Sciences, Asan Medical Center, Seoul, Korea.

Conflict of Interest

J.L. reports a relationship with VN Inc. that includes: board membership and equity or stocks. The remaining authors declare no conflict of interest.

Data Availability Statement

The data that support the findings of this study are available from the corresponding author upon reasonable request.

Keywords

adhesion, anti-migration, hydrogels, mechanical interlocking, network-like porous layer, stents

Received: October 1, 2024
Revised: February 18, 2025
Published online: March 12, 2025

[1] a) H. Sung, J. Ferlay, R. L. Siegel, M. Laversanne, I. Soerjomataram, A. Jemal, F. Bray, *CA Cancer J. Clin.* **2021**, *71*, 209; b) J.-H. Park, H. Y. Song, J. H. Kim, H. Y. Jung, J. H. Kim, S. B. Kim, H. Lee, *Am. J. Roentgenol.* **2012**, *199*, 1380; c) R. T. Ripley, I. S. Sarkaria, R. Grosser, C. S. Sima, M. S. Bains, D. R. Jones, P. S. Adusumilli, J. Huang, D. J. Finley, V. W. Rusch, N. P. Rizk, *Ann. Thorac. Surg.* **2016**, *101*, 226.

[2] W. Dudzic, C. Płatkowski, M. Folwarski, J. Meyer-Szary, K. Kaźmierczak-Siedlecka, M. Ekman, T. Wojciechowicz, M. Dobosz, *Nutrients* **2023**, *15*, 1524.

[3] a) N. C. M. van Heel, J. Haringsma, H. Boot, A. Cats, S. A. L. W. Vanhoutvin, E. J. Kuipers, *Gastrointest. Endosc.* **2012**, *76*, 52; b) M. K. Wilson, S. R. Carr, *Ann Esophagus* **2023**, *6*; c) A. Fugazza, A. Capogreco, A. Repici, *Tech. Innovations Gastrointest. Endosc.* **2020**, *22*, 192; d) R. B. Perumpail, V. R. Muthusamy, *Tech. Innovations Gastrointest.Endosc.* **2020**, *22*, 239.

[4] P. Hindy, J. Hong, Y. Lam-Tsai, F. Gress, *Gastroenterol Hepatol.* **2012**, *8*, 526;

[5] a) P. Sharma, R. Kozarek, A. C. Gastroenterology, *Am. J. Gastroenterol.* **2010**, *105*, 258; b) T. H. Baron, *New Engl. J. Med.* **2001**, *344*, 1681; c) P. D. Siersema, *Nat. Clin. Pract. Gastroenterol. Hepatol.* **2008**, *5*, 142.

[6] a) H. Mozafari, P. Dong, S. Zhao, Y. Bi, X. Han, L. Gu, *Comput. Biol. Med.* **2018**, *100*, 43; b) J.-H. Park, H. Y. Song, J. H. Shin, Y. C. Cho, J. H. Kim, S. H. Kim, J. Park, *Am. J. Roentgenol.* **2015**, *204*, 1109; c) G. Schiavone, S. P. Lacour, *Sci. Transl. Med.* **2019**, *11*, aaw5858; d) X. Liu, Y. Yang, M. E. Inda, S. Lin, J. Wu, Y. Kim, X. Chen, D. Ma, T. K. Lu, X. Zhao, *Adv. Funct. Mater.* **2021**, *31*, 2010918.

[7] a) B. C. Martins, F. A. Retes, B. F. Medrado, M. S. de Lima, C. M. Pennacchi, F. S. Kawaguti, A. V. Safatle-Ribeiro, R. S. Uemura, F. Maluf-Filho, *World J. Gastrointest. Endosc.* **2014**, *6*, 49; b) J.-H. Park, H. Y. Song, J. Y. Park, J. H. Kim, Y. H. Kim, J. H. Kim, S. B. Kim, *Eur. Radio.* **2013**, *23*, 1940.

[8] a) H. K. Na, H. Y. Song, J. H. Kim, J. H. Park, M. K. Kang, J. Lee, S. J. Oh, *Eur. Radiol.* **2013**, *23*, 786; b) J.-S. Ji, B. I. Lee, H. K. Kim, Y. S. Cho, H. Choi, B. W. Kim, S. W. Kim, S. S. Kim, H. S. Chae, K. Y. Choi, L. S. Maeng, *Gastrointest. Endosc.* **2011**, *74*, 148; c) C. S. Shim, Y. D. Cho, J. H. Moon, J. O. Kim, J. Y. Cho, Y. S. Kim, J. S. Lee, M. S. Lee, *Endoscopy* **2001**, *33*, 843; d) E. M. Verschuur, E. W. Steyerberg, E. J. Kuipers, P. D. Siersema, *Gastrointest. Endosc.* **2007**, *65*, 592; e) E. S. Kim, S. W. Jeon, S. Y. Park, C. M. Cho, W. Y. Tak, Y. O. Kweon, S. K. Kim, Y. H. Choi, *J. Gastroenterol. Hepatol.* **2009**, *24*, 114.

[9] a) E. M. L. Verschuur, M. Y. Homs, E. W. Steyerberg, J. Haringsma, P. J. Wahab, E. J. Kuipers, P. D. Siersema, *Gastrointest. Endosc.* **2006**, *63*, 134; b) M. J. Uitdehaag, P. D. Siersema, M. C. Spaander, F. P. Vleggaar, E. M. Verschuur, E. W. Steyerberg, E. J. Kuipers, *Gastrointest. Endosc.* **2010**, *71*, 600; c) G. Vanbiervliet, J. Filippi, B. S. Karimdjee, N. Venissac, A. Iannelli, A. Rahili, E. Benizri, D. Pop, P. Staccini, A. Tran, S. Schneider, J. Mouroux, J. Gugenheim, D. Benchimol, X. Hébuterne, *Surg. Endosc.* **2012**, *26*, 53; d) J. W. Kim, S. Lee, D. S. Ryu, J. Park, H. Lee, H. K. Na, J. H. Noh, D. H. Kim, J. H. Park, H. Y. Jung, K. Na, *Biomaterials* **2023**, *299*, 122159; e) S. V. Kantsevoy, M. Bitner, *Gastrointest. Endosc.* **2012**, *76*, 1251.

[10] a) M. K. Gangwani, H. Haghbin, Z. Ahmed, A. Aziz, M. Aziz, W. M. Lee-Smith, D. S. Dahiya, Y. Nawras, F. Kamal, S. Inamdar, Y. Alastal, D. G. Adler, *Am. J. Gastroenterol.* **2023**, *118*, S964; b) M. Schiemer, D. Bettinger, J. Mueller, M. Schultheiss, H. Schwacha, P. Hasselblatt, R. Thimme, A. Schmidt, A. Kuellmer, *Gastrointest Endosc* **2022**, *96*, 1; c) E. Rieder, C. M. Dunst, D. V. Martinec, M. A. Cassera, L. L. Swanstrom, *Endoscopy* **2012**, *44*, 1121; d) R. Law, A. Prabhu, L. Fujii-Lau, C. Shannon, S. Singh, *Surg. Endosc.* **2018**, *32*, 675; e) E. I. Chang, M. G. Galvez, J. P. Glotzbach, C. D. Hamou, S. El-ftesi, C. T. Rappleye, K. M. Sommer, J. Rajadas, O. J. Abilez, G. G. Fuller, M. T. Longaker, G. C. Gurtner, *Nat. Med.* **2011**, *17*, 1147.

[11] S. Nam, D. Mooney, *Chem. Rev.* **2021**, *121*, 11336.

[12] a) H. Choi, Y. Kim, S. Kim, H. Jung, S. Lee, K. Kim, H. S. Han, J. Y. Kim, M. Shin, D. Son, *Nat. Electron.* **2023**, *6*, 779; b) B. Xue, J. Gu, L. Li, W. T. Yu, S. Yin, M. Qin, Q. Jiang, W. Wang, Y. Cao, *Nat. Commun.* **2021**, *12*, 7156; c) J. Wu, H. Yuk, T. L. Sarrafian, C. F. Guo, L. G. Griffiths, C. S. Nabzdyk, X. Zhao, *Sci. Transl. Med.* **2022**, *14*, abh2857; d) J. Deng, H. Yuk, J. J. Wu, C. E. Varela, X. Y. Chen, E. T. Roche, C. F. Guo, X. Zhao, *Nat. Mater.* **2021**, *20*, 229.

[13] J. Li, A. D. Celiz, J. Yang, Q. Yang, I. Wamala, W. Whyte, B. R. Seo, N. V. Vasilyev, J. J. Vlassak, Z. Suo, D. J. Mooney, *Science* **2017**, *357*, 378.

[14] X. Liu, C. Steiger, S. Lin, G. A. Parada, J. Liu, H. F. Chan, H. Yuk, N. V. Phan, J. Collins, S. Tamang, G. Traverso, X. Zhao, *Nat. Commun.* **2019**, *10*, 493.

[15] J. Deng, H. Yuk, J. J. Wu, C. E. Varela, X. Y. Chen, E. T. Roche, C. F. Guo, X. H. Zhao, *Nat. Mater.* **2021**, *20*, 229.

[16] a) M. A. Rahman, C. Bowland, S. R. Ge, S. R. Acharya, S. Kim, V. R. Cooper, X. C. Chen, S. Irle, A. P. Sokolov, A. Savara, T. Saito, *Sci. Adv.* **2021**, *7*, abk2451; b) M. G. Mazzotta, A. A. Putnam, M. A. North, J. J. Wilker, *J. Am. Chem. Soc.* **2020**, *142*, 4762; c) Z. Pan, Q. Q. Fu, M. H. Wang, H. L. Gao, L. Dong, P. Zhou, D. D. Cheng, Y. Chen, D. H. Zou, J. C. He, X. Feng, S. H. Yu, *Nat. Commun.* **2023**, *14*, 5378.

[17] J. H. Li, Q. Q. Dai, Z. Wang, Y. Z. Yi, Y. Shen, Z. W. Yao, S. C. Niu, Z. W. Han, L. Q. Ren, *Adv. Mater.* **2024**, *36*, 2406432.

[18] X. Yao, J. J. Liu, C. H. Yang, X. X. Yang, J. C. Wei, Y. Xia, X. Y. Gong, Z. G. Suo, *Adv. Mater.* **2019**, *31*, 1903062.
[19] a) E. Jeon, J. M. Kang, G. H. Bae, C. H. Zeng, S. Shin, B. Lee, W. Park, J. H. Park, J. Lee, *Adv. Healthcare Mater.* **2022**, *11*, 2200389; b) H. Jung, S. H. Park, J. Lee, B. Lee, J. Park, Y. Seok, J. H. Choi, M. G. Kim, C. S. Song, J. Lee, *Anal. Chem.* **2021**, *93*, 792; c) E. Jeon, B. Koo, S. Kim, J. Kim, Y. N. Yu, H. Jang, M. J. Lee, S. H. Kim, T. J. Kang, S. K. Kim, R. Kwak, Y. Shin, J. S. Lee, *Nat. Commun.* **2024**, *15*, 1366.
[20] Z. Liu, Z. Liu, S. Ji, G. Wang, *Sci. Rep.* **2020**, *10*, 16750.
[21] C. Y. Zhang, H. Xie, Y. Du, X. L. Li, W. L. Zhou, T. Wu, J. P. Qu, *Adv. Funct. Mater.* **2023**, *33*, 2213398.
[22] a) J.-A. Park, S.-C. Lee, S.-B. Kim, *J. Mater. Sci.* **2019**, *54*, 9969; b) R. Ellerbrock, M. Stein, J. Schaller, *Sci. Rep.* **2022**, *12*, 11708.
[23] D. M. Fitzgerald, Y. L. Colson, M. W. Grinstaff, *Nat. Rev. Mater.* **2023**, *8*, 3.
[24] S. Rose, A. Prevoteau, P. Elzière, D. Hourdet, A. Marcellan, L. Leibler, *Nature* **2014**, *505*, 382.
[25] a) J. Liu, S. Lin, X. Liu, Z. Qin, Y. Yang, J. Zang, X. Zhao, *Nat. Commun.* **2020**, *11*, 1071; b) X. Shi, L. Zhu, H. Yu, Z. Tang, S. Lu, H. Yin, M. You, G. Sun, Q. Chen, *Adv. Funct. Mater.* **2023**, *33*, 2301036.
[26] R. Panigrahi, S. Chakraborty, J. Ye, G. S. Lim, F. C. H. Lim, J. K. H. Yam, L. Y. Wu, S. Chng, M. Prawirasatya, A. M. van Herk, P. Thoniyot, *Macromol. Rapid Commun.* **2020**, *41*, 2000240.
[27] a) M. Zhang, Z. Gao, K. Hakobyan, W. Li, Z. Gu, S. H. Peng, K. Liang, J. Xu, *Small* **2024**, *20*, 2310572; b) D. Won, H. Kim, J. Kim, H. Kim, M. W. Kim, J. Ahn, K. J. Min, Y. S. Lee, S. K. Hong, J. Choi, C. Y. Kim, T. S. Kim, S. H. Ko, *Nat. Electron.* **2024**, *7*, 475.
[28] a) V. V. Khutoryanskiy, *Macromol. Biosci.* **2011**, *11*, 748; b) A. H. C. Anthis, X. Q. Hu, M. T. Matter, A. L. Neuer, K. C. Wei, A. A. Schlegel, F. H. L. Starsich, I. K. Herrmann, *Adv. Funct. Mater.* **2021**, *31*, 2007099.
[29] S. Cai, C. Wu, W. Yang, W. Liang, H. Yu, L. Liu, *Nanotechnol. Rev.* **2020**, *9*, 971.
[30] a) G. Tian, D. Yang, C. Liang, Y. Liu, J. Chen, Q. Zhao, S. Tang, J. Huang, P. Xu, Z. Liu, D. Qi, *Adv. Mater.* **2023**, *35*, 2212302; b) L. Xu, S. Gao, Q. Guo, C. Wang, Y. Qiao, D. Qiu, *Adv. Mater.* **2020**, *32*, 2004579.
[31] a) K. Y. Kim, J. Tsauo, H. Y. Song, P. H. Kim, J. H. Park, *J Korean Med. Sci.* **2017**, *32*, 1062; b) H. K. Na, H. Y. Song, J. H. Kim, J. H. Park, M. K. Kang, J. Lee, S. J. Oh, *Eur. Radiol.* **2013**, *23*, 786.
[32] a) C. S. Shim, *Clin. Endosc.* **2012**, *45*, 235; b) J. H. Park, H. Y. Song, J. Y. Park, J. H. Kim, Y. H. Kim, J. H. Kim, S. B. Kim, *Eur. Radiol.* **2013**, *23*, 1940; c) J. H. Kim, H. Y. Song, E. K. Choi, K. R. Kim, J. H. Shin, J. O. Lim, *Eur. Radiol.* **2009**, *19*, 384.
[33] a) M. Carrancá, L. Griveau, N. Remoué, C. Lorion, P. Weiss, V. Orea, D. Sigaudo-Roussel, C. Faye, D. Ferri-Angulo, R. Debret, J. Sohier, *J. Biomed. Mater. Res., Part A* **2021**, *109*, 926; b) Q. S. Liu, A. Chiu, L. H. Wang, D. An, W. C. Li, E. Y. Chen, Y. Zhang, Y. Pardo, S. P. McDonough, L. Y. Liu, W. F. Liu, J. Chen, M. L. Ma, *Biomaterials* **2020**, *230*, 119640.
[34] a) J. H. Kim, H. Y. Song, J. H. Park, H. J. Yoon, H. G. Park, D. K. Kim, *Radiology* **2010**, *255*, 75; b) J. H. Park, T. H. Kim, Y. C. Cho, N. Bakheet, S. O. Lee, S. H. Kim, K. Y. Kim, *Cardiovasc. Interventional Radiol.* **2019**, *42*, 1343; c) J.-H. Park, W. Park, S. Cho, K. Y. Kim, J. Tsauo, S. H. Yoon, W. C. Son, D.-H. Kim, H.-Y. Song, *ACS Appl. Mater. Interfaces* **2018**, *10*, 29357.
[35] M. K. Wilson, S. R. Carr, *Ann. Esophagus* **2021**, *6*, 18.
[36] Y. Chen, P. Gao, L. Huang, X. Tan, N. Zhou, T. Yang, H. Qiu, X. Dai, S. Michael, Q. Tu, N. Huang, Z. Guo, J. Zhou, Z. Yang, H. Wu, *Nat. Commun.* **2021**, *12*, 7079.
[37] E.-Y. Kim, J. H. Shin, Y. Y. Jung, D.-H. Shin, H.-Y. Song, *J. Vasc. Interventional Radiol.* **2010**, *21*, 1287.
[38] E. J. Jun, J.-H. Park, J. Tsauo, S.-G. Yang, D.-K. Kim, K. Y. Kim, M. T. Kim, S.-H. Yoon, Y. J. Lim, H.-Y. Song, *Gastrointest. Endosc.* **2017**, *86*, 219.